

Single crystal plasticity defies bulk-phase mechanics in Isoniazid cocrystals with analogous cofomers

Jay Prakash A. Yadav, Ram Naresh Yadav, Praveer Sihota, Hongbo Chen, Chenguang Wang, Changquan Calvin Sun, Navin Kumar, Arvind K Bansal, and Sanyog Jain

Cryst. Growth Des., **Just Accepted Manuscript** • DOI: 10.1021/acs.cgd.9b00247 • Publication Date (Web): 26 Jun 2019

Downloaded from <http://pubs.acs.org> on July 1, 2019

Just Accepted

“Just Accepted” manuscripts have been peer-reviewed and accepted for publication. They are posted online prior to technical editing, formatting for publication and author proofing. The American Chemical Society provides “Just Accepted” as a service to the research community to expedite the dissemination of scientific material as soon as possible after acceptance. “Just Accepted” manuscripts appear in full in PDF format accompanied by an HTML abstract. “Just Accepted” manuscripts have been fully peer reviewed, but should not be considered the official version of record. They are citable by the Digital Object Identifier (DOI®). “Just Accepted” is an optional service offered to authors. Therefore, the “Just Accepted” Web site may not include all articles that will be published in the journal. After a manuscript is technically edited and formatted, it will be removed from the “Just Accepted” Web site and published as an ASAP article. Note that technical editing may introduce minor changes to the manuscript text and/or graphics which could affect content, and all legal disclaimers and ethical guidelines that apply to the journal pertain. ACS cannot be held responsible for errors or consequences arising from the use of information contained in these “Just Accepted” manuscripts.

Single crystal plasticity defies bulk-phase mechanics in Isoniazid cocrystals with analogous cofomers

Jay Prakash Yadav¹, Ram Naresh Yadav², Praveer Sihota², Hongbo Chen³, Chenguang Wang³, Changquan Calvin Sun³, Navin Kumar², Arvind Bansal^{1*}, Sanyog Jain^{1*}

¹ Department of Pharmaceutics, National Institute of Pharmaceutical Education and Research (NIPER), S.A.S. Nagar - 160 062, Punjab, INDIA

² Department of Mechanical Engineering, Centre of Materials Science and Energy Engineering, Indian Institute of Technology (IIT) Ropar, Rupnagar - 140 001, Punjab, INDIA

³ Pharmaceutical Materials Science and Engineering Laboratory, Department of Pharmaceutics, College of Pharmacy, University of Minnesota, Minneapolis, MN - 55455, USA

*Corresponding Authors

Dr. Sanyog Jain

Associate Professor, Centre for Pharmaceutical Nanotechnology, Department of Pharmaceutics,

National Institute of Pharmaceutical Education and Research (NIPER),

Sector 67, S.A.S. Nagar - 160 062, Punjab, India.

Email: sanyogjain@niper.ac.in,

Contact No: +91-172-2292055, Fax No.: +91-172-2214692

Prof. Arvind K. Bansal

1
2
3 Head, Department of Pharmaceutics, National Institute of Pharmaceutical Education and
4
5 Research (NIPER),
6

7 Sector 67, S.A.S. Nagar - 160 062, Punjab, India.
8

9 E-mail address: akbansal@niper.ac.in,
10

11 Contact No. +91-172- 2214682, Fax No.: +91-172-221469
12
13
14
15
16
17
18
19
20
21
22
23
24
25
26
27
28
29
30
31
32
33
34
35
36
37
38
39
40
41
42
43
44
45
46
47
48
49
50
51
52
53
54
55
56
57
58
59
60

Abstract

Crystal structure of four INZ cocrystals with analogous cocrystal formers were probed to understand the relationships among molecular packing, H-bonding dimensionality, single crystal plasticity and bulk mechanical behavior. These structurally analogous cofomers coherently directed H-bonds by ‘philic’ functionalities (—OH and —COOH) and vdW interactions by ‘phobic’ scaffold ($\text{—C}_6\text{H}_{(5-n)}$, where $n = \text{—OH}$). Compared to INZ:2HBA and INZ:4HBA, INZ:BA and INZ:GA exhibited higher plasticity and hence, better tableting performance due to larger bonding area and higher tensile strength. The rank order of apparent yield pressure and incipient plasticity quantified from “In-die” Heckel analysis of bulk phase $\text{INZ:2HBA} > \text{INZ:4HBA} > \text{INZ:GA} > \text{INZ:BA}$ however, does not match that of nanomechanical hardness and elastic modulus $\text{INZ:BA} > \text{INZ:2HBA} > \text{INZ:4HBA} > \text{INZ:GA}$. The discrepancy may be attributed to the anisotropy in crystal mechanical properties, where the stiffness of the dominant crystal faces probed with nanoindentation may grossly deviate to the bulk mechanical behavior. Therefore nanomechanical attributes are more predictive of more isotropic molecular crystals, such as 3D H-bonded or interlocked structures, than those exhibiting gross structural anisotropy, such as crystals with distinct molecular layers that favor facile slip. Hence accurate prediction of bulk behavior based on nanomechanical characterization requires incorporation of crystal shape and packing as well as knowledge of facet specific mechanical properties. Moreover, prediction of bonding strength based on molecular packing still remains warranted wherein crystallographic molecular slip may cause deviation in proposed relationship.

Keywords: Analogous cofomers, basic structural motif, molecular slip, crystal plasticity, dihedral angle, H-bonding dimension

Introduction

Accurate prediction of bulk phase performance from crystal structure requires the correlation between molecular level crystal structure-function mechanics and their macroscopic properties.¹ It has been shown that crystal structure influence the physicochemical and mechanical properties.^{1, 2} Chemical nature also significantly influences solid-state properties, as shown by multi-component systems, like cocrystals.¹ A combinatorial approach of supramolecular chemistry and crystal engineering,³ therefore, plays a crucial role in modifying, or designing crystal properties, including mechanical property,^{1, 4} of crystalline phase to attain desired properties.⁵⁻⁸ In fact, a modification of mechanical properties, such as plasticity,⁹ elasticity, and fracture behavior, by crystal engineering adopting multi-component approach, such as using cocrystallization,^{1, 4, 10} is an effective way to modulate tableting behavior.¹¹ The efforts made to understand the bending behavior in molecular crystal¹² and highly flexible, elastic crystal was also designed in polyhalogenated compound.¹³ There have been a review by Naumov and co-workers which describes mechanically responsive molecular crystals wherein actuation is achieved by external factors such as light irradiation, heat, mechanical force or other stimuli.¹⁴ Moreover, cocrystallization confers the way to tune the mechanical property for desired performance. The impact of cocrystallization on crystal properties depends on the modularity by extent and exchange of native property of partner molecules after forming a supramolecular assembly. Cocrystallization can improve^{10, 11} or deteriorate¹⁵ mechanical behavior in comparison to crystals of parent molecules.^{16, 17} Mechanical properties of a cocrystal do not necessarily depend on those of the cofomers. Thus, the use of cocrystallization to improve solubility of active pharmaceutical ingredient (API), by using soluble cofomers,^{18, 19-21} may inadvertently compromise mechanical behavior and other pharmaceutically important properties. As a result, the selection of a suitable cocrystal for

1
2
3 drug development requires clear understanding of impact of crystal structure on all
4 properties of interest. Understanding the intricacies among crystal structure, crystal
5 mechanical properties, and bulk tableting performance,^{22, 23} still remains challenging.
6
7

8
9 It is generally accepted that the facile activation of slip mechanism under the mechanical
10 stress confers plastic (irreversible) deformation²⁴ and usually offers higher tensile strength
11 by increasing interparticulate bonding area.²⁵ However, successful prediction of bulk
12 deformation from crystal structure is not always possible.²⁶ Crystals without known
13 structural features that facilitate facile plastic deformation, such as absence of flat
14 molecular layers nor bending columns, exhibited superior mechanical behavior.²²
15
16 Designing plastic crystal structure with desired mechanical properties for a given API may
17 not always be possible, despite the significant advancement of crystal engineering,^{3, 6}
18
19 More work is needed to both better understand crystal – bulk mechanical performance
20 relationship and more effectively design crystals with desired properties. Such
21 supramolecular translation from single crystal response to bulk phase behavior remains
22 elusive. In this direction, we have examined the relationships among crystal structure,
23 crystal mechanical properties using four cocrystals of an API, Isoniazid (INZ), with four
24 analogous cofomers. The common molecular features of these analogous cofomers
25 include polar/hydrophilic ($-\text{OH}$)_n (n = 0, 1, 3) and $-\text{COOH}$ and non-polar/hydrophobic
26 ($-\text{C}_6\text{H}_{(5-n)}$), systematic variation of which are expected to influence molecular packing in
27 crystals with both directional H-bonds and non-directional van der Waals interactions.
28
29 This system offers an opportunity to probe how these four basic distinct structural variants
30 of molecular packing accommodate stress at nano-scale level, e.g. initiation of crystal
31 plastic deformation. Such hierarchy or behavioral interplay of may guide the design of
32 other multi-component molecular crystals.
33
34
35
36
37
38
39
40
41
42
43
44
45
46
47
48
49
50
51
52
53

54 **Experimental Section**

Materials

Isoniazid (INZ) was purchased from Wockhardt Ltd., Mumbai, India. Benzoic acid (BA), Salicylic acid (2HBA), *p*-OH BA (4HBA) and Gallic acid (GA) were of analytical grade (AR) and purchased from S.D. Fine-Chem. Ltd., Mumbai, India. Methanol (J.T. Bakers, Gliwice, Poland), Ethanol and Acetonitrile (Merck Life sciences Pvt. Ltd., Mumbai, India) used in crystallization experiment were of HPLC grade.

Methods

Crystallization of Molecular Solids

A 1:1 stoichiometric ratio of INZ with cofomers BA, 2HBA, 4HBA and GA (3, 4, 5-tri HBA or TBA) was used to prepare cocrystals as per the reported methods.²⁷⁻²⁹ They were added into 250 mL round bottom flask and dissolved in methanol for preparing INZ:2-HBA, INZ:4-HBA and INZ:GA,^{28, 29} and 2:1 v/v mixture of Ethanol:Acetonitrile for INZ:BA.²⁷ Solutions were refluxed at 60 ± 2.0 °C while stirring for 60 min. The clear solution was cooled to room temperature (26 ± 2.0 °C) and resultant clear solution was allowed to slowly evaporate at ambient condition. Prism (INZ:GA), plate (INZ:4-HBA and INZ:BA), and needle-to-plate (INZ:2-HBA) shape cocrystals were obtained and dried at 45 ± 2.0 °C in an oven for 3 h. The bulk quantity was scaled-up to 2 g.

Powder X-ray diffraction

PXRD patterns of all cocrystals were recorded at room temperature (25.0 ± 2.0 °C) on a Bruker's D8 Advance Diffractometer (Bruker, AXS, Karlsruhe, Germany) with Cu K α radiation (1.54 Å), at 40.0 kV, 40.0 mA passing through Nickel (Ni) filter. Analysis was performed in a continuous mode with a step size of 0.01° and step time of 1 s over an angular range of 4.0 to 40.0° 2θ scale. The recorded powder X-ray diffractograms were

1
2
3 further analyzed by DIFFRAC plus EVA software (version 9.0, Bruker, AXS, Karlsruhe,
4 Germany) and compared with respective simulated or calculated PXRD pattern.

7 **Differential scanning calorimetry**

8
9
10 Thermal analysis was performed using DSC (Q2000, TA Instruments, New Castle, DE,
11 USA) operating with Universal Analysis[®] software, version v4.5A. About 4-5 mg of each
12 solid was weighed accurately in aluminum pans and heated at the heating rate of 10
13 °C·min⁻¹. During analysis, dry nitrogen (N₂) purge was maintained at 50 mL·min⁻¹. The
14 instrument was calibrated using high purity standard of indium before sample analysis.
15
16
17
18
19

20 **Particle size distribution**

21
22
23 Similar particle size fraction of all samples was obtained by sieving using BSS# sieves.
24
25 D₅₀ and D₉₀ of all samples were further determined by optical light microscope based on
26 size along the longest axis, for at least 300 particles (DMLP microscope, Leica
27 Microsystems, Wetzlar, Germany).
28
29
30
31

32 **Moisture content**

33
34
35 Moisture content of all samples (accurately weighed about 500 mg) was estimated by
36 Karl Fischer titration (Metrohm 794 basic titrino, Herisau, Switzerland). The
37 instrument was calibrated with disodium tartrate dihydrate before measuring samples (n
38 = 3).
39
40
41
42
43
44

45 **Bulk and true density determination**

46
47
48 Bulk density (ρ_b) was estimated by carefully adding accurately weighed powder to a
49 10.0 mL measuring cylinder. The true density (ρ_t) of all molecular solids was
50 determined in triplicate (n = 3) by Helium pycnometry (Pycno 30, Smart Instruments,
51 Mumbai, India) under ambient conditions (25.0 ± 2.0 °C/40.0 ± 5.0 % RH).
52
53
54
55
56
57
58
59
60

Specific surface area analysis

Specific surface area (SSA) of powder samples was determined using Nitrogen gas sorption (SMART SORB 91 Surface area analyzer, Smart instruments, Mumbai, India). The instrument was first calibrated by injecting a known quantity of Nitrogen. The measured parameters were further used to calculate the SSA of all samples by employing Brunauer, Emmett and Teller (BET) equation. 500 mg of each sample was placed into the glass loop of the instrument and then submerged into liquid N₂. The quantity of the adsorbed N₂ gas was measured using thermal conductivity detector and further integrated using electronic circuit. The reported values are mean (average) of the three measurements (n=3).

Nanoindentation experimentation

Nanoindentation was performed on oriented single crystals of all molecular solids using a Ti-950 TriboIndenter (Hysitron Inc., Minneapolis, MN, USA) equipped with Berkovich diamond tip. A tripyramidal (Berkovich) tip with an included angle of 142.3° and a tip radius of ~150 nm was employed for indentations. The tip area function was calibrated using fused silica and polycarbonate standards. The testing temperature was 28 ± 0.5 °C and relative humidity was 45 ± 5 %. The regions for testing were identified using an optical microscope integrated into the nanoindentation system. The “tip to optics calibration” was done by performing 10 indents in “H-pattern”. For area function calibration, a series of indents with different contact depths were performed on a standard sample of known elastic modulus (*E*). A plot of the calculated area as a function of contact depth (*h*) was created and fitted by the TriboScan software. For quasi-static analysis of all samples, 11-12 subsequent indents were performed along the length midline parallel to the longest axis of crystal on a dominant face with user-specified parameters. Indentations

with contact depths of an order of magnitude larger than local surface roughness are thought to be sufficiently deep to avoid a strong effect of roughness on the measured mechanical properties. Peak load (P) for these indentations was 2000 μN and indent spacing was 55.0 μm . A load function consisting of a 5 s loading to peak force (F) segment, followed by a 2 s hold segment and a 5 s unloading segment was used (the loading and unloading rates were 0.4 mN s^{-1}). The nanomechanical hardness (H) and the elastic modulus (E_r) were computed employing the Oliver and Pharr's method.³⁰ The E_r is related to the Young's modulus of Elasticity of tested sample (E_s) and the indenter (E_i) through the following relationship:

$$\frac{1}{E_r} = \frac{(1 - \nu_i^2)}{E_i} + \frac{(1 - \nu_s^2)}{E_s} \quad \text{Equation 1}$$

Where, ν_i and ν_s are the Poisson's ratio (ν) for the indenter and the substrate materials, respectively. The value of elastic modulus and Poisson's ratio for the diamond indenter tip are 1140 GPa and 0.07, respectively, for diamond indenter tip.

Dynamic hydraulic compression analysis

In order to generate the load-displacement profile (and stress-strain ($\check{S} - \hat{S}$) curve), samples were tested on an "in-die" compressive set-up using closed-loop hydraulic dynamic compression testing machine (Servo-Pulser, 4830, Shimadzu) with a capacity of maximum achievable load of 5.290 kN. The loading platens and compressive set-up are made of hard steel and have fine-polished surfaces. Accurately weighed powder sample (400 mg) of each solid was compressed with a single loading method in a load control mode with a rate of 0.5 kN/s and data sampling interval was of 0.1 second. The initial height of powder sample was used to calculate strain of the powder bed. Two calibrated linear variable differential transformers (LVDTs) were used to measure the axial

1
2
3 displacement. The load, F and axial displacement were continually monitored and
4
5 recorded.

8 **Preparation of compacts**

9
10 For collecting “out-of-die” compressibility, tableability, and compactibility profiles,
11
12 tablets were compressed at varied compaction pressures of 50, 100, 150, 200 and 300 MPa
13
14 separately on a Materials Testing Machine (Model 1485, Zwick-Roell, Ulm, Germany)
15
16 using 6 mm flat tip round B-tooling. The tableting speed was kept at 4 mm min⁻¹. Punch
17
18 tips and die wall were brushed with a suspension of magnesium stearate in ethanol (5%
19
20 w/v) and dried with a fan before each compaction test. For “in-die” Heckel analysis,
21
22 powdered materials were compressed up to compaction pressure of 200 MPa using the
23
24 same experimental set-up as that described in “out-of-die” analysis.
25
26
27
28

29 **Calculation of tablet tensile strength and porosity**

30
31 Breaking force (F) of all the compacts was measured using a texture analyzer (TA-XT2i,
32
33 Texture Technologies Corp., Scarsdale, NY) at a speed of 0.01 mm/s. Tablet dimensions
34
35 were measured using a digital caliper (CD-6 CS, Digimatic Mitutoyo Corporation, Japan).
36
37 Tensile strength (σ) was calculated using equation (2) to eliminate the undesirable effect
38
39 of variable compact thickness (t) on measured F .
40
41

$$42 \quad \sigma = \frac{2F}{\pi dt} \quad \text{Equation 2}$$

43
44
45 Where, σ is the tensile strength (MPa), F is the observed breaking force (N), d is the
46
47 diameter (mm), and t is the thickness of the compact (mm). The porosity, ε , of the
48
49 compacts was calculated using equation (3).
50
51

$$52 \quad \varepsilon = 1 - \frac{\rho_c}{\rho_t} \quad \text{Equation 3}$$

Where, ρ_c is the density of tablet calculated from the weight and volume of the resulting compact. ρ_t is the true density (ρ_t) of the powder.

Statistical analysis

Statistical significance for values of various nanomechanical and bulk deformation parameters was compared using a two tailed paired *t*-test using commercial software (SigmaStat version 3.5, San Jose, CA, USA), and the parameters were considered to be statistically significant if $P < 0.05$.

Molecular modeling

The crystal structures were analyzed for relative arrangement of molecules and differences in their inter-molecular interactions, H-bonding dimensionality, using CSD-Enterprise's module Mercury software (Version 3.9 CCDC, Reg. No. 800579, UK).

The dispersion-corrected density functional theory model used for estimating intermolecular interactions was shown to be accurate. The pair wise intermolecular interaction energy was estimated using CrystalExplorer V.17 and Gaussian09W with experimental crystal geometry. The hydrogen positions normalized to standard neutron diffraction values were used during the calculation. For each molecule in the asymmetric unit of a crystal, the total intermolecular interaction energy with another molecule, calculated using the B3LYP-D2/6-31G(d,p) electron densities model, is the sum of electrostatic, polarization, dispersion, and exchange-repulsion components with scaling factors of 1.057, 0.740, 0.871, and 0.618, respectively. The intermolecular interaction is ignored with molecule - molecule distance more than 3.8 Å. For cocrystal with asymmetric unit contains a drug and one coformer. The interaction energies of drug and coformer with neighboring molecules were separately calculated. The interlayer or intralayer interaction energies were calculated by adding interaction energies between a

given molecule in one layer and all interacting molecules in a neighboring layer or within the same layer, respectively. The interaction energies below a certain energy threshold (10 kJ/mol) are omitted for clarity, and resultant cylinder thickness is proportional to the intermolecular interaction energies in the respective lattice.³¹

Results and Discussion

Interpretation of crystal structure: Molecular aspects of analogous cocrystal cofomers (aCCFs)

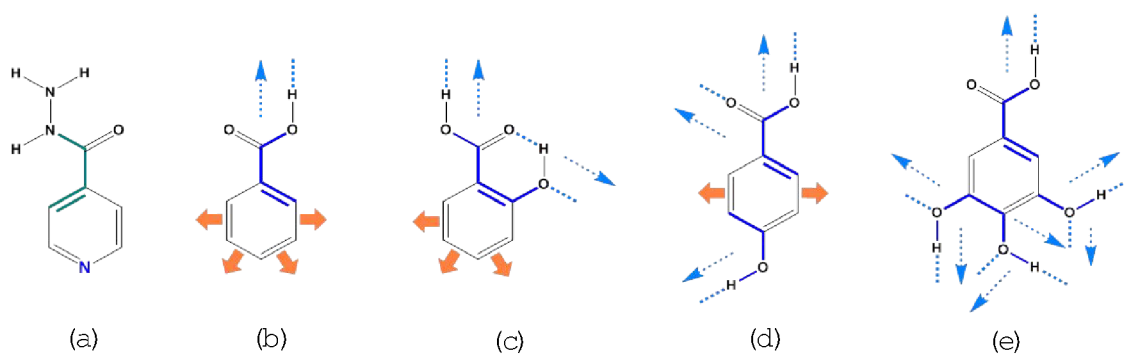


Figure 1. Molecular structure of (a) INZ and analogous cofomers; (b) Benzoic acid (BA), (c) 2HBA (*o*-OH BA), (d) 4HBA (*p*-OH BA), (e) Gallic acid (3,4,5-triOH BA). Cofomers present schematically intermolecular interactions in crystal lattice with INZ; H-bonds vector (interaction motif: blue-dotted arrows) from polar (—OH and —COOH; ‘philic’) functionalities and vdW interactions (packing motif: orange solid arrows) from non-polar (‘phobic’) aromatic scaffold. The torsion angles are cyan-colored in INZ and blue in cofomers.

Figure 1 illustrates molecular structures, intermolecular interaction vectors (both directional H-bonds and non-directional vdW) and related torsion angles associated with INZ and cofomers. The “philic” —OH is absent in Benzoic acid (BA)($n = 0$), but present in 2HBA, 4HBA and TBA. These additional —OH groups direct relative orientation of INZ, through intermolecular H-bonds in cocrystals. The 3 —OH groups on the planer Gallic acid (GA) obscure most part of the “phobic” aromatic ring (Figure 1e)

to make it much more polar. The polarity of 2HBA and 4HBA falls in between BA and GA, where *o*- position to 2HBA and leaves more exposed aromatic ring than 4HBA to favor more non-specific vdW interactions (Figure 1c and 1d). The nitrogen to the INZ interacts with —COOH forming a robust primary acid···pyridine chain, *C*(4), synthon. The acid···pyridine *C*(4) dominates in many

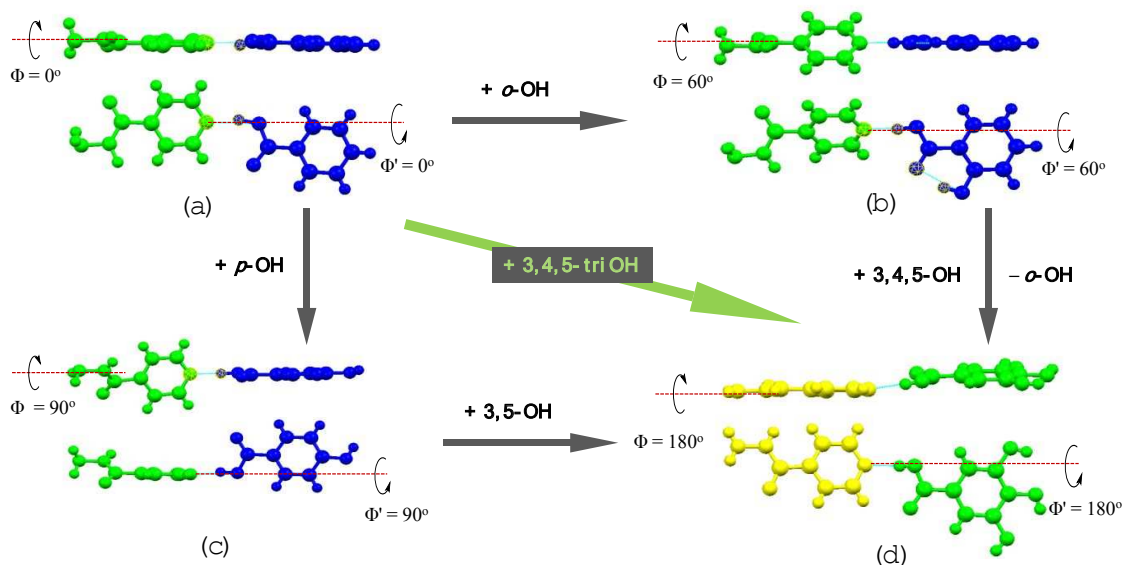


Figure 2-a. The relative orientation of INZ (green, and yellow in (d)) with respect to coformers (blue, and green in (d)) displayed by dihedral angle (Φ) around robust primary synthon acid···pyridine *C*(4) in the crystallographic plane. $\Phi = 0^\circ = 180^\circ$ dictates coplanarity of both molecules, $\Phi = 90^\circ$ perpendicularity (\perp) and $\Phi = 60^\circ$ relatively tilted orientation/inclination of aromatic moiety. The colors have been assigned by symmetry equivalence mode in molecular packing. (a) INZ:BA, (b) INZ:2HBA, (c) INZ:4HBA, (d) INZ:GA

other variants of coformer molecular packing (not discussed here). It is hence referred as primary synthon. To better understand this robust primary synthon, relative torsion and orientation of INZ and coformers are explored for co-planarity between INZ and coformers (Figure 2-a). The *o*- or *p*- —OH directs not only orientation of INZ, but also $\pi\cdots\pi$ stacking and overall molecular packing (Figures 3 and 4). The relative orientation of

INZ around acid \cdots pyridine synthon preferentially controls homo- and heteromolecular hydrophobic $\pi\cdots\pi$ stacking interactions between cofomers and INZ. Maximal isotropic vdW interactions are prevalent into both extremities i.e. INZ:BA and INZ:GA (Figure 4a and 4b). Crystal structure of INZ:BA with $\pi\cdots\pi$ is chiral,^{27, 32, 33} which forms herringbone H-bonded column wherein homomolecular BA $\pi\cdots\pi$ interactions are pointed outwards and homomolecular INZ $\pi\cdots\pi$ interactions are inwards (Figure 4a).

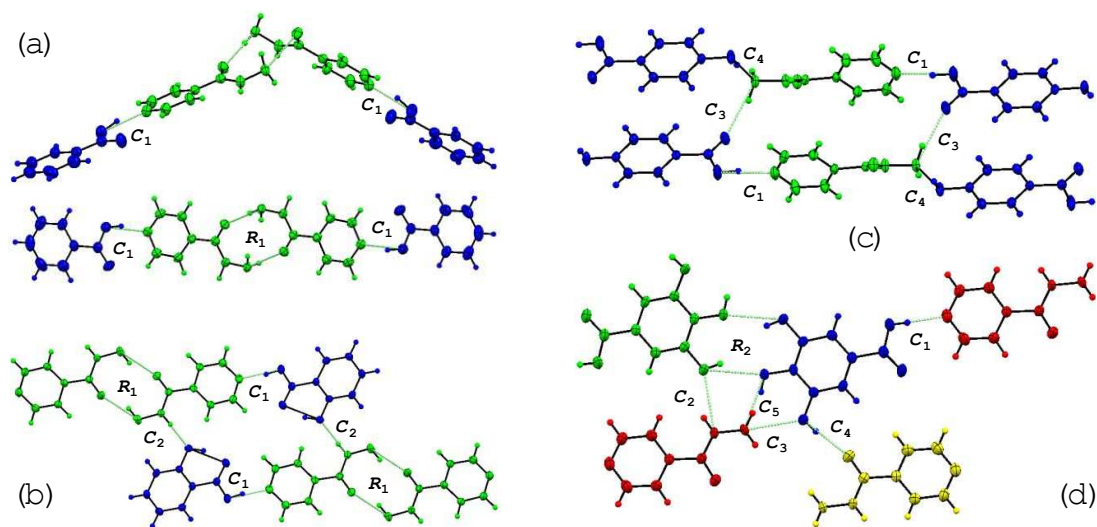


Figure 2-b. Analysis of unit structural H-bonded motifs (USHbMs) with primary (1°) and secondary (2°) synthons in molecular packing of (a) INZ:BA, (b) INZ:2HBA, (c) INZ:4HBA and (d) INZ:GA. Common synthon(s) is designated by same subscripted integer number (S_N). Robust 1° synthon acid \cdots pyridine (C_1) is common for all packing, homosynthon R_1 visualized in both (a) and (b). Except (d), rests of all USHbMs (a, b, c) are interacted centro-symmetrically, whereas non-centrosymmetrically interacted INZ:GA (d) possess distinct ring motif R_2 and chain synthons C_4 and C_5 .

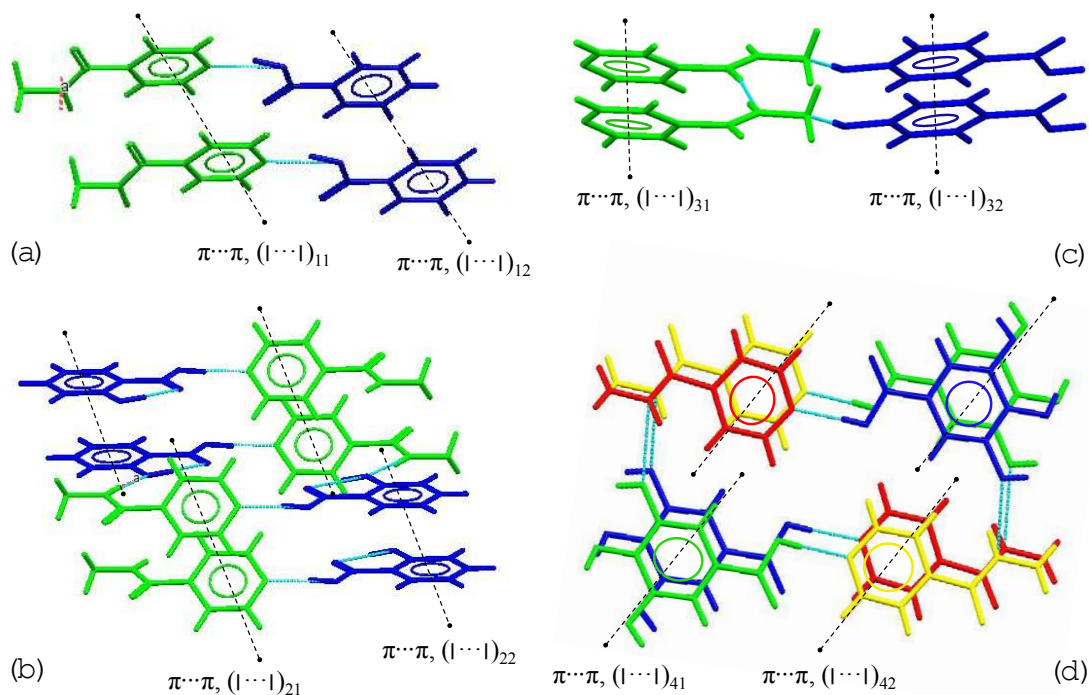


Figure 3. Visualization of homomolecular (cohesive) $\pi\cdots\pi$ stacking ($|\cdots|$) interactions in basic structural motifs/BSMs ((a) INZ:BA and (c) INZ:4HBA) and among adjacent molecular layers ((b)INZ:2HBA and (d)INZ:GA). No heteromolecular (adhesive) $|\cdots|$ interactions. For two subscripted integer numbers, initial presents respective system, for e.g. 1-(a), 2-(b), 3-(c), 4-(d), whereas subsequent second integer is generalized as 1 for INZ and 2 for respective analogous coformer.

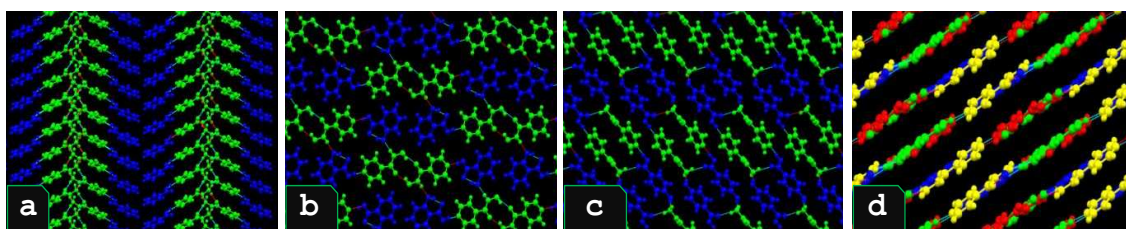


Figure 4. Molecular packing of INZ cocrystals with BA and —OH substituted coformers. (a) INZ:BA, 2D H-bonded columns with tilted aromatic rings of INZ and BA forming ‘brush’ like columnar structure (along crystallographic c -axis), (b) INZ:2HBA with 2D H-bonded near close-pack structure with interspersed H-bonds and vdW interactions (along b -axis), (c) INZ:4HBA, 2D H-bonded columnar-layered chains (vdW interactions between layers and H-bonds within chains; along b -axis), (d) INZ:GA, 2D H-bonded layered slip system (visualized along b -axis).

1
2
3 The 3 —OH groups to GA enforce a layered structure having vdW interactions between
4 the planes and H-bonds within the planes. Such kind of $\pi\cdots\pi$ interactions do not form at
5 the expense of H-bond between —OH and primary and/or secondary —NH₂ of hydrazide
6 functionality into molecular packing of INZ:2-HBA and INZ:4-HBA (Figure 4b and 4c).
7
8 The same kind of co-planarity does exist for INZ and GA (Figure 2), but only
9 homomolecular $\pi\cdots\pi$ interactions are present between INZ and GA (Figure 3). The only
10 difference between BA and GA is the absence and presence of polar —OH functionality
11 attached to the aromatic ring, respectively. Hence, block of directional H-bond extension
12 forms bending columnar packing in INZ:BA, but continuous extension of H-bonds from
13 crystallographic planes in INZ:GA. Molecular packing of INZ:2HBA is near anisotropic
14 (3D) close-pack with 1D H-bonded chains (Figure 4b). On the other hand, INZ:4HBA
15 forms columnar-layered structure having 1D H-bonded chain as primary basic structural
16 motif (BSM) and layer as a secondary BSM (Figure 4c). Here, BSMs are referring to
17 structure features having the highest molecular density, consisting of an assembly of H-
18 bonded molecules in the structure, which is flanked by layers of vdW interactions.
19
20
21
22
23
24
25
26
27
28
29
30
31
32
33
34
35

36 **Nano-scale level deformation: Quantifying single crystal plasticity (η_{cr})**

37
38 The experimental X-ray diffraction patterns of the cocrystal single crystals were in good
39 agreement with their respective calculated powder X-ray diffraction patterns (supporting
40 information). Figure 5a shows representative load-displacement curves, and 5b and 5c
41 show E and H values, respectively. All recorded $L-h$ profile were smooth, without any
42 displacement burst (known as “pop-in”). The continuous crystal deformation associated
43 with smooth profiles indicated, the presence of multiple active slip systems. Figure 6c
44 demonstrates the maximal depth of tip penetration during loading (hc_1) and unloading
45 (hc_2). Nanomechanical parameter E quantifies strength of materials against reversible
46 elastic deformation and is dependent on intermolecular interactions and molecular
47
48
49
50
51
52
53
54
55
56
57
58
59
60

packing efficiency and relative orientation of molecular plane with respect to the indentation load. On the other hand, H is a measure of material strength against irreversible plastic deformation, which is dependent on the relative ease for molecular slippage to occur along specific crystallographic plane(s). Both E and H depend on orientation of indenting axis relative to molecular slip plane(s).

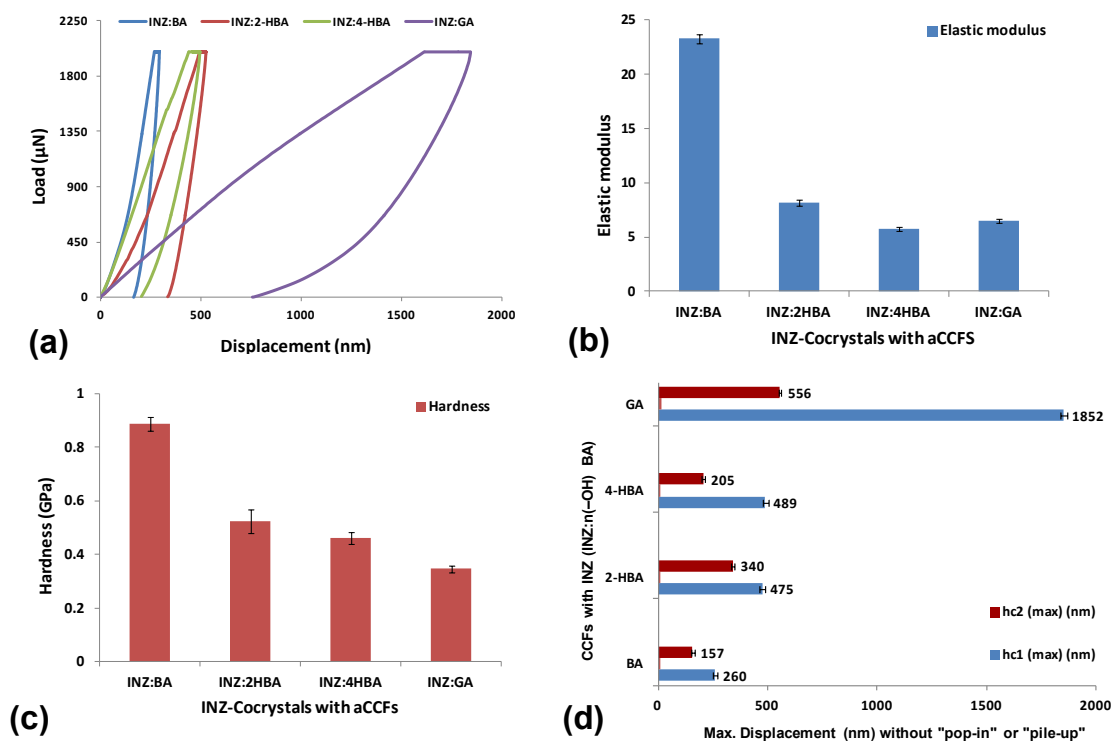


Figure 5. a) Representative load-displacement ($L-h$) curves (without any “pop-in”/“displacement bursts” during loading). (b and c) Nanomechanical attributes: Young’s modulus of Elasticity (E , GPa), and Hardness (H , GPa). (d) Maximum depth of penetration/displacement (nm) during loading (hc_1) and unloading (hc_2) event.

The anisotropic, molecular packing patterns in four cocrystals can be characterized by the means of BSM. The BSM in INZ:BA is columnar. BSM in INZ:2HBA consists of near isotropic close-pack structure. On the other hand, INZ:4HBA is the columnar-layered crystal, wherein primary BSM is chains, which are further connected by H-bonds to form a layer of secondary BSM. INZ:GA crystallizes as shearing solids having layered

BSM consisting of obvious crystallographic slip planes. E, H, hc₁ and hc₂ can be rationalized by molecular crystal plasticity,

$$E(hc_2), f(x) \approx \frac{W(x)_{BSM}}{W(x)_{(vdW)\infty}} + [(E_{att}) \cdot \cos \theta] \quad \text{Equation 4}$$

$$H(hc_1), f(x) \approx \frac{W(x)_{(vdW)\infty}}{W(x)_{BSM}} + [(E_{att}) \cdot \cos \theta] \quad \text{Equation 5}$$

where, W_{BSM} is the width of 1D/2D H-bonded BSMs, W_{(vdW) ∞} is the distance of separation between the BSM by infinite vdW interactions or largest *d*-spacing in case of multiple slip system, E_{att} is the attachment energy or interaction energy between adjacent BSM. θ is the angular resolution between the BSM (or least E_{att} crystallographic plane) and the direction of applied mechanical load. Energy framework analysis of molecular packing and characteristic BSM help to understand the nanomechanical behavior. Table 1 and 2 enumerates possible primary (and secondary) crystallographic slip system with its topological nature along which low energy molecular slips are considered to be occurred.

Table 1. Topological analysis of crystallographic slip system

Crystal Form	refcode	Plane	Unobstructed	Separation (+)/interdigitation (-)	Orthogonal Planes (>45°)
INZ-2HBA	LATKUO	(0 0 2)	Yes	0.94	Yes
INZ-4HBA	FADHEZ	(1 0 -2)	Yes	0.78	Yes
INZ-BA	SETRIU	(1 0 0)	Yes	1.2	No
INZ-GA	LODHOD02	(0 0 1)	Yes	2.06	No

Table 2. Identification of primary crystallographic (low energy molecular) slip planes

hkl	Multiplicity	d_{hkl}	Surface area	E_{att}(Total)	Distance (Å)	% Total facet area
INZ-BA						
{ 1 0 0}	2	25.80554	23.84238	-5.48067	5.480667	84.56277
INZ-2HBA						
{ 0 0 2}	2	14.88521	42.24323	-35.2221	35.22209	50.17179
INZ-4HBA						
{ 1 0 0}	2	12.90157	101.4396	-67.3364	67.33639	35.01775
INZ-GA						
{ 0 0 1}	2	13.21285	99.96984	-49.0132	49.01322	42.49636

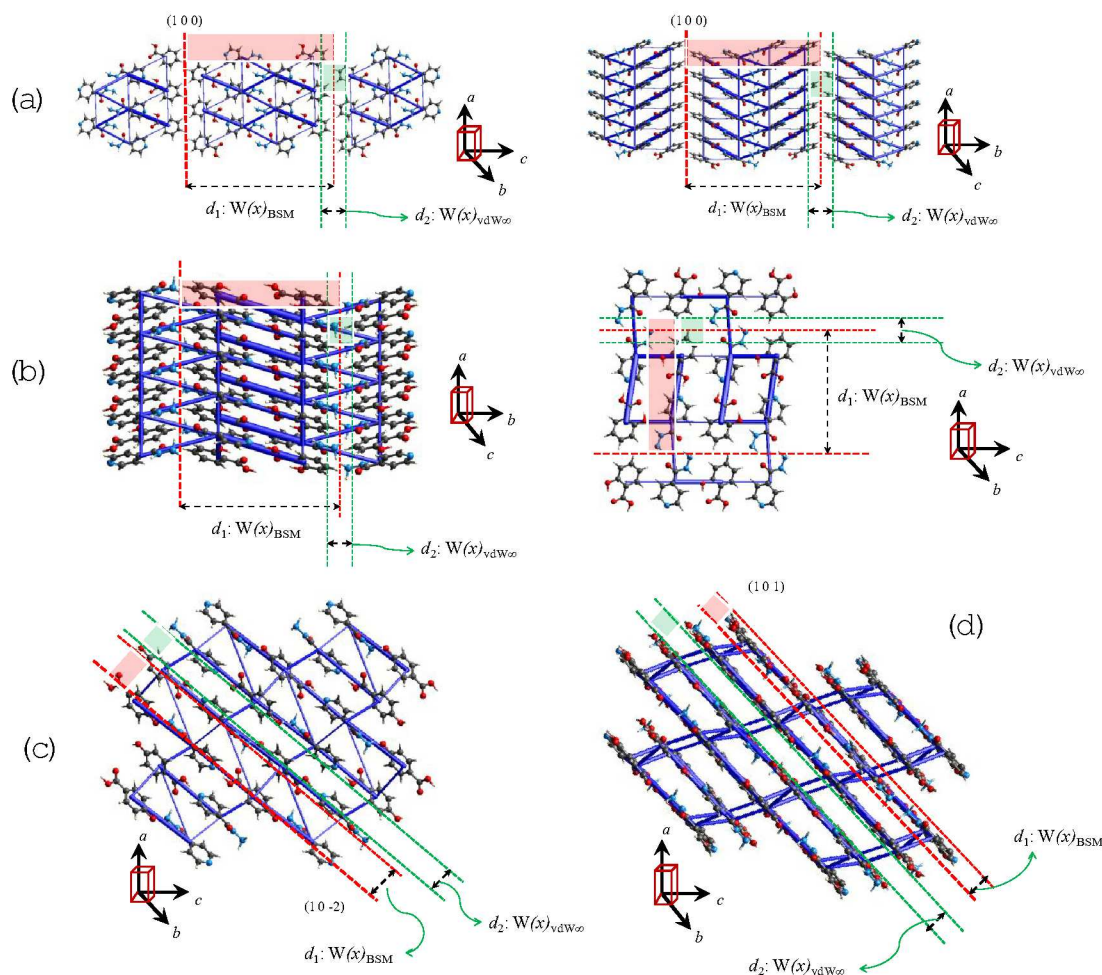


Figure 6. Energy framework analysis and visualization of BSM along primary crystallographic planes. (a) INZ:BA, lack of strong interlayer interaction indicated the possible bending behavior and $(1\ 0\ 0)$ is primary slip plane. (b) INZ:2HBA, 3D more isotropic interaction bonding energy. (c) INZ:4HBA and (d) INZ:GA have similar layered structure, the molecular layers expanded along $(1\ 0\ -2)$ for INZ:4HBA and $(1\ 0\ 1)$ for INZ:GA. Due to the interlayer interaction, the plasticity of both could be lower than INZ:BA. Higher d_1/d_2 corresponds to higher E and H , while Higher d_2/d_1 is related with lower E and H when $\theta \approx 0$ or minimum.

In case of INZ:BA, lack of strong interactions between adjacent BSM satisfies the criteria for possible molecular slip (Figure 6a). INZ:2HBA revealed more isotropic (3D) bonding energy interactions (Figure 6b). While INZ:4HBA and INZ:GA both being more anisotropic, demonstrated interlayer interactions when expanded along respective

crystallographic plane (Figure 6c and 6d). The crystal stiffness quantified by E and H follows the descending order of INZ:BA > INZ:2HBA > INZ:4HBA > INZ:GA. The tip displacement (hc_1 and hc_2) at the same indentation load followed the reverse order of stiffness.

The identification of strong directional H-bonds fortified BSM enables prediction of possible molecular slip.⁴ INZ:BA with columnar BSM resists molecular slip having higher $W(x)_{\text{BSM}}$ but lower of $W(x)_{(\text{vdW})\infty}$ (indented face (010), identified molecular slip along $\langle 010 \rangle$). The columnar BSMs, being effective at short or even large distance of separation would resist deformation and provided larger E , H values and lower loading and unloading displacement (Figure 5). At the other extreme, the shearing INZ:GA crystal, exhibiting lower $W(x)_{\text{BSM}}$ but higher $W(x)_{(\text{vdW})\infty}$, was found to be relatively plastic solid ($\langle 101 \rangle$, (001)). In other words, BSMs spanning large distance of separation by infinite vdW interactions, as projected along a specific crystallographic plane, could facilitates considerable plastic deformation when indented or stretched beyond their elastic limit.

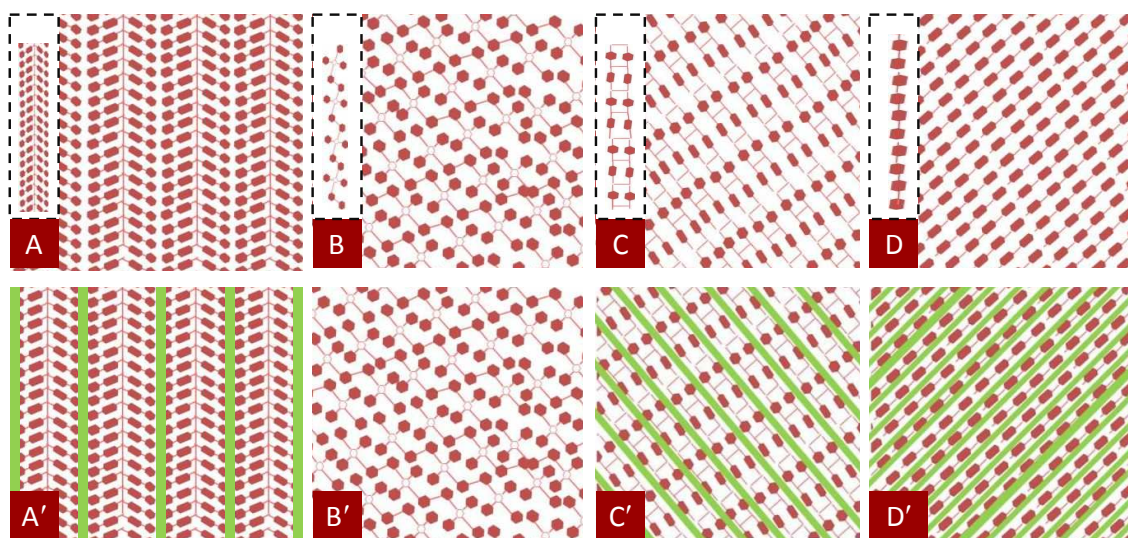


Figure 7-a. Schematic representation of molecular packing, descendent of Figure 4, projecting along the same crystallographic axis in the context of BSM (red) flanked by weak vdW interactions (green lines).

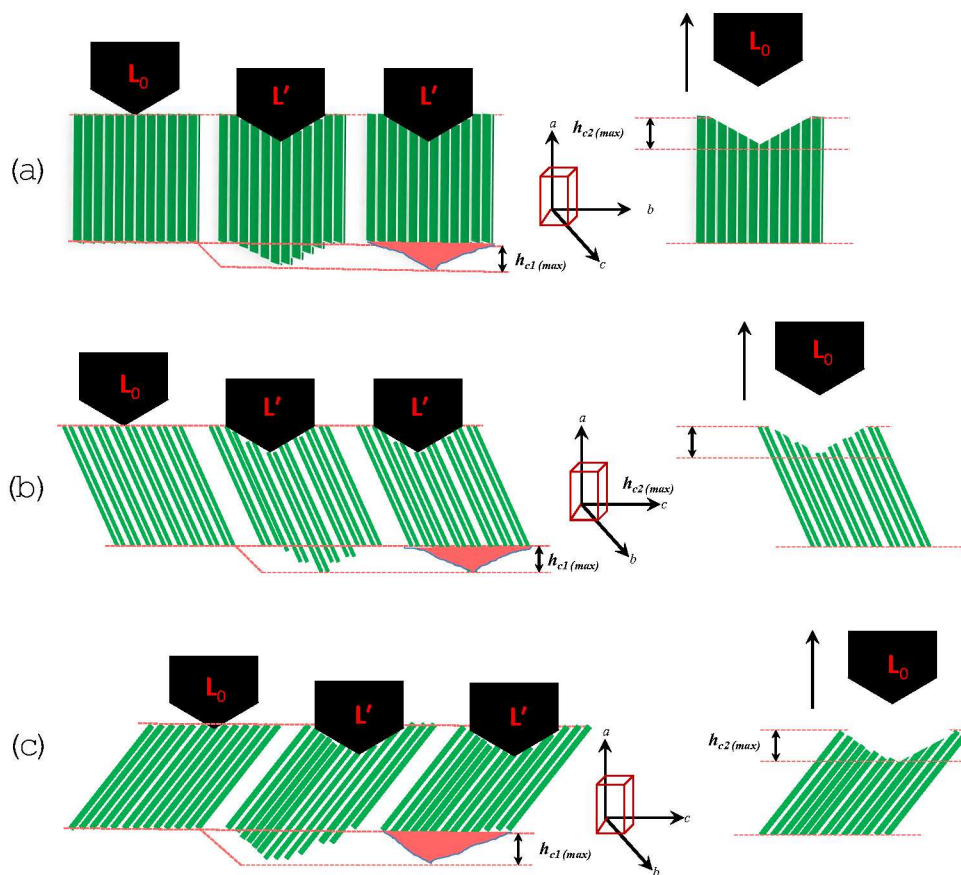


Figure 7-b. Schematic depiction of nano-scale level viscoelastic deformation mechanism understood in the context of nature of BSM and identified (low energy) molecular slip. (a) - Figure 7-a, (A/A'), (b) - (C/C'), (c) - (D/D'). Displacement during loading (h_{c1} , plasto-elastic deformation) and unloading (h_{c2} , plastic deformation). Where, $L' - L_0 = 2000 \mu\text{N}$.

The INZ:2HBA and INZ:4HBA crystals have the intermediate nature of $W(x)_{\text{BSM}}$ and $W(x)_{(\text{vdW})\infty}$ and hence are expected to possess intermediate values of E , H , hc_1 and hc_2 . In case of INZ:4HBA, possible molecular slip was identified as $\langle -102 \rangle$ (indented face (100)). INZ:2HBA has near isotropic 3D close-pack molecular packing, active molecular slip can be identified along $[002]$ ($\{200\}$) without breakage of any weak H-bonding interactions. Moreover, post-indentation restoration or recovery depends reciprocally on

$W(x)_{(vdW)\infty}$, hence the degree of recovery was $INZ:BA > INZ:2HBA > INZ:4HBA > INZ:GA$. The nature of this nano-scale level deformation behavior is schematically presented in the context of BSM ($W(x)_{BSM}$ and $W(x)_{(vdW)\infty}$) in Figure 7-a and 7-b.

Bulk-phase mechanical behavior

In an attempt to correlate molecular level structural features with bulk performance, particle level parameters such as particle size distribution, specific surface area and moisture content were controlled to comparable values for all samples (supporting information). Figure 8a represents stress-strain curve and plastic energy of the solids as a function of applied compaction stress. Interestingly, at the peak stress of 39.35 ± 0.04 MPa, the maximum strain followed the order of $INZ:BA - 0.467 \pm 0.05$ MPa > $INZ:GA - 0.393 \pm 0.03$ MPa \approx $INZ:2HBA - 0.391 \pm 0.03$ MPa > $INZ:4HBA - 0.318 \pm 0.01$ MPa. Counter-intuitively, the most stiff $INZ:BA$ demonstrated the highest strain (46.7%). $INZ:2HBA$ and $INZ:GA$ showed nearly the same strain, despite their significantly different nanomechanical stiffness. Straightforward translation from the nanomechanical behavior to bulk phase behavior was observed only for $INZ:4HBA$ only.

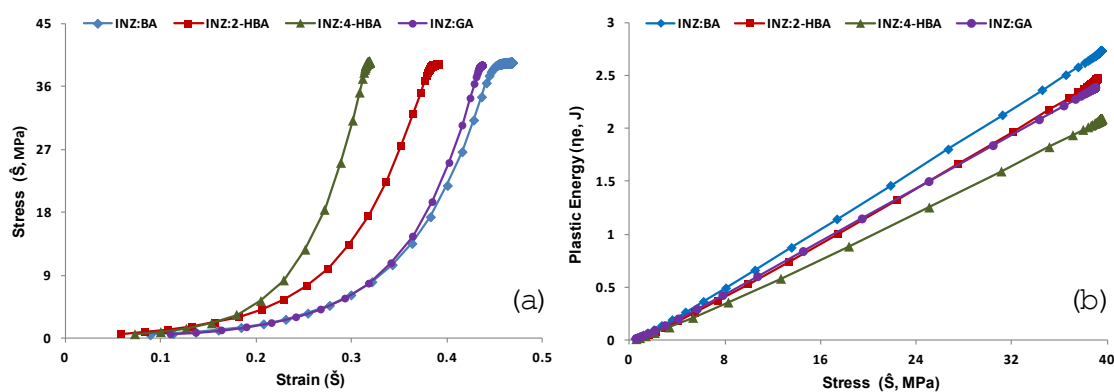


Figure 8. Bulk mechanical behavior of $INZ:BA$, $INZ:2HBA$, $INZ:4HBA$, and $INZ:ADP$ obtained from hydraulic dynamic compression analysis: (a) Stress-strain profile, and (b) Plastic Energy versus stress (MPa) relationship.

Plastic energy increased gradually as the stress was raised for all the solids (Figure 8b). However, comparatively the most stiff solid INZ:BA having higher E and H values, had highest plastic energy (2.74 ± 0.07 J). The two systems having similar strain also have comparable plastic energy (2.47 ± 0.05 J and 2.38 ± 0.06 J) tendency at the applied stress, while the lowest plastic energy was found for (INZ:4HBA, 2.07 ± 0.03 J). Therefore, the rank order of nanomechanical parameters did not correlate well with the order of their bulk level strain-stress behavior as well as plastic energy of the system.

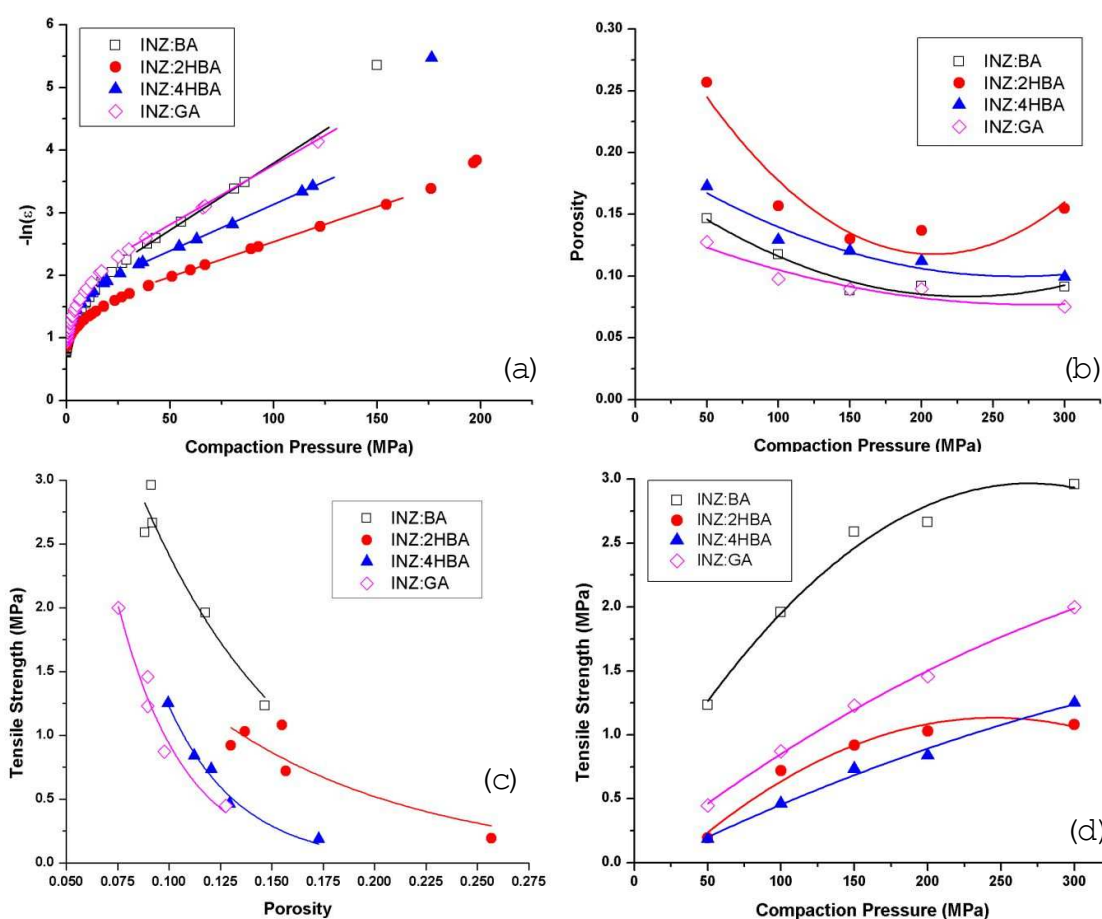


Figure 9. Bulk mechanical behavior: (a) "In-die" Heckel analysis, "Out-of-die" bulk CTC profile, (b) Compressibility (Bonding Area), (c) Compactibility (Bonding Strength), and (d) Tableability obtained as a function of applied compaction pressure.

However, E and H correlated better with the apparent mean yield pressure (P_y) derived from "In-die" Heckel analysis. For all materials, "In-die" porosity (ϵ) decreased

1
2
3 gradually in all cases as expected (Figure 9a). “In die” Heckel analysis accounts both
4 plastic as well as elastic deformation. It, therefore, provides a more realistic assessment
5 of powder properties under a load than “out-of-die” analysis. The P_y values follow the
6 descending order of INZ:2HBA (81.3 ± 5.7 MPa), followed by INZ:4HBA (67.8 ± 5.7
7 MPa) > INZ:GA (54.3 ± 1.3 MPa) > INZ:BA (45.0 ± 0.4 MPa). It seems that moderately
8 stiffer solids possess higher P_y , whereas rest of INZ:BA and INZ:GA yielded lower P_y .
9 Hence higher/lower E and H values have been still correlated well with higher/lower
10 value of P_y , except INZ:GA. Because of the critical role of plastic deformation and
11 elastic recovery in the “Out-of-die” CTC (Compressibility, Tabletability, Compactibility)
12 profiles, H is expected to correlate with them.
13

14 Compactibility can be used to assess interparticulate bonding strength (BS), where
15 apparent BS may be quantified by σ at the zero ϵ . Interestingly, plastic solids had higher
16 apparent BS than stiffer ones. Whereas tensile strength (σ_0) measured for compacts
17 followed the order of INZ:4HBA (22.0 ± 6.4 MPa) > INZ:GA (20.9 ± 7.8 MPa) > INZ: BA
18 (9.1 ± 2.3 MPa) > INZ:2HBA (4.0 ± 2.8 MPa). Higher σ_0 was found in case of solids
19 having lower E and H , and comparatively higher E and H lead to lower σ_0 . In general,
20 materials having lower E and H are more deformable. The curve is less steeper for
21 INZ:2HBA and INZ:4HBA, and steeper for INZ:BA and INZ:GA (Figure 9a), which
22 generally corresponds to their relative E and H .
23

24 Compressibility provides a means to assess interparticulate bonding area (BA) and is
25 related with plasticity of material. Other things being equal, larger average BA is
26 expected in a tablet with a lower porosity. Hence, at the same compaction pressure, BA
27 follows the descending order of INZ:GA > INZ:BA > INZ:4HBA > INZ:2HBA (Figure
28 9b), which however deviated from their respective stiffness as measured by H and E .
29 Under a given compaction pressure, the lower porosity achieved in crystals with slip
30
31
32
33
34
35
36
37
38
39
40
41
42
43
44
45
46
47
48
49
50
51
52
53
54
55
56
57
58
59
60

1
2
3 system and columnar BSM crystals (e.g. INZ:GA and INZ:BA), but porosity is higher in
4
5 cases of columnar-layered and more anisotropic crystals INZ:4HBA and INZ:2HBA
6
7 crystals, respectively. Thus the layered/columnar crystal structure exhibits higher both
8
9 BA and BS, which explains its highest tableability (Figure 9d). Tensile strength
10
11 increased gradually as the stress was raised, however, tableting is higher in case of
12
13 INZ:BA and INZ:GA as compared to INZ:2HBA and INZ:4HBA. This behaviour can be
14
15 rationalized by BA-BS interplay, where BA contributions to tablet tensile strength of
16
17 stiffer materials is less. Consistent with the observation by Hewitt, lower H/E yields
18
19 better compaction behavior in this work, where the lower H/E (INZ:BA: 0.038)
20
21 corresponds to both highest compressibility (BA) and tableability than other cocrystal
22
23 (INZ:2HBA: 0.064, INZ:4HBA: 0.079, INZ:GA: 0.053).
24
25
26

27 28 **Conclusion**

29
30 This study explored the mechanical behavior of multi-component cocrystals formed with
31
32 analogous cofomers, where crystal structure analyses offered insights into their
33
34 nanomechanical behavior. A correlation can be made by considering the nature of
35
36 BSM and separation distance by infinite vdW interactions, low energy molecular slip and
37
38 the loading directions. Bulk mechanical behavior is an average outcome arising from
39
40 random orientation of particle deformation. The 3D H-bonded more isotropic close-pack
41
42 INZ:2HBA and 2D columnar-layered structure INZ:4HBA with comparatively inactive
43
44 molecular slip correlated well with their bulk performance. The translation of
45
46 nanomechanical behavior to bulk deformation performance is, however, unreliable for
47
48 anisotropic cocrystal with layered H-bond fortified crystallographic planes. Lack of
49
50 information about facets specific indentation experimentation is owing to nature of
51
52 samples and crystal habit, hence it can be limitation. Other factors, such as crystal lattice
53
54 defects and crystal fracture, remain to be considered for reliable prediction of bulk phase
55
56
57
58
59
60

1
2
3 behavior. Hence, accurate prediction of bulk mechanical behavior based on single-site
4 calculation and molecular packing remains a challenge, and therefore, each material
5 needs to be investigated on a case-to-case basis. The impact of anisotropy on mechanical
6 properties and bulk behavior requires more in-depth understanding to develop a robust
7 corelationship among crystal structure, nanomechanical property, and bulk compaction
8 behavior.
9
10
11
12
13
14
15
16

17 **Supporting information**

18
19 The Powder X-ray diffraction (PXRD) patterns, DSC heating curves (meting point and
20 heat of fusion), and particle and bulk level characterization (Table S-1), of the studied
21 molecular solids have been enclosed as supporting information (ESI) of this work.
22
23
24
25
26
27

28 **References**

- 29
30
31 1. Reddy, C. M.; Krishna, G. R.; Ghosh, S., Mechanical properties of molecular crystals
32 - applications to crystal engineering. *CrystEngComm* **2010**, 12, (8), 2296-2314.
- 33
34 2. Shariare, M. H.; Leusen, F. J. J.; de Matas, M.; York, P.; Anwar, J., Prediction of the
35 mechanical behaviour of crystalline solids. *Pharmaceutical research* **2012**, 29, (1),
36 319-331.
- 37
38 3. Moulton, B.; Zaworotko, M. J., From molecules to crystal engineering:
39 supramolecular isomerism and polymorphism in network solids. *Chemical Reviews*
40 **2001**, 101, (6), 1629-1658.
- 41
42 4. Varughese, S.; Kiran, M.; Ramamurty, U.; Desiraju, G. R., Nanoindentation in crystal
43 engineering: Quantifying mechanical properties of molecular crystals. *Angewandte*
44 *Chemie International Edition* **2013**, 52, (10), 2701-2712.
- 45
46 5. Desiraju, G. R., Supramolecular synthons in crystal engineering—a new organic
47 synthesis. *Angewandte Chemie International Edition in English* **1995**, 34, (21), 2311-
48 2327.
- 49
50 6. Desiraju, G. R., Crystal engineering: from molecule to crystal. *Journal of the*
51 *American Chemical Society* **2013**, 135, (27), 9952-9967.
52
53
54
55
56
57
58
59
60

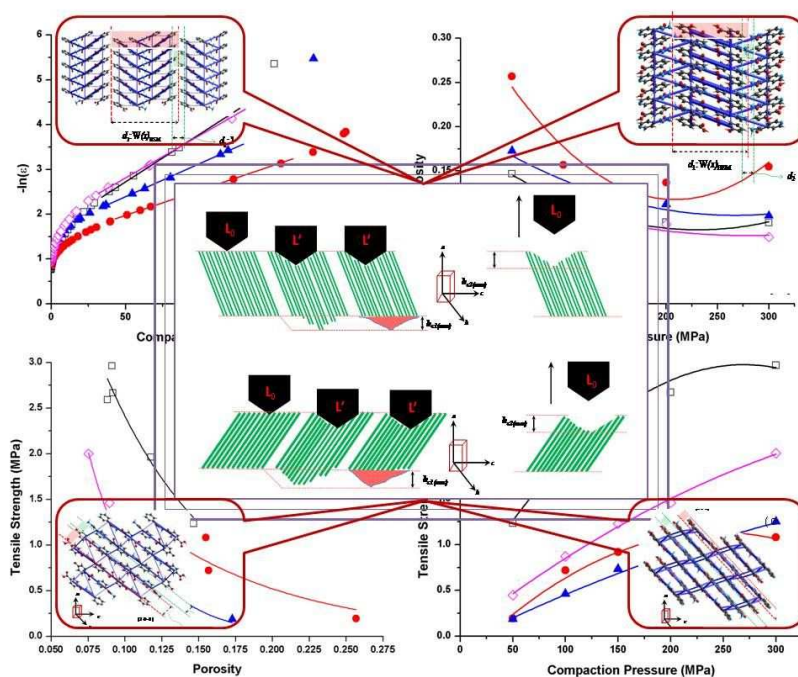
- 1
- 2
- 3 7. Aakeroy, C. B.; Beatty, A. M., Crystal engineering of hydrogen-bonded assemblies-a
- 4 progress report. *Australian journal of chemistry* **2001**, 54, (7), 409-421.
- 5
- 6 8. Lehn, J. M., Perspectives in supramolecular chemistry“from molecular recognition
- 7 towards molecular information processing and self“organization. *Angewandte*
- 8 *Chemie International Edition* **1990**, 29, (11), 1304-1319.
- 9
- 10 9. Chang, S.-Y.; Sun, C. C., Superior plasticity and tabletability of theophylline
- 11 monohydrate. *Molecular pharmaceutics* **2017**, 14, (6), 2047-2055.
- 12
- 13 10. Sun, C. C.; Hou, H., Improving mechanical properties of caffeine and methyl gallate
- 14 crystals by cocrystallization. *Crystal Growth and Design* **2008**, 8, (5), 1575-1579.
- 15
- 16 11. Karki, S.; FriÅ;Ä□iÄ;†, T.; Fabian, L.; Laity, P. R.; Day, G. M.; Jones, W., Improving
- 17 mechanical properties of crystalline solids by cocrystal formation: new compressible
- 18 forms of paracetamol. *Advanced materials* **2009**, 21, (38â€□39), 3905-3909.
- 19
- 20 12. Reddy, C. M.; Gundakaram, R. C.; Basavoju, S.; Kirchner, M. T.; Padmanabhan, K.
- 21 A.; Desiraju, G. R., Structural basis for bending of organic crystals. *Chemical*
- 22 *Communications* **2005**, (31), 3945-3947.
- 23
- 24 13. Ghosh, S.; Mishra, M. K.; Kadambi, S. B.; Ramamurty, U.; Desiraju, G. R., Designing
- 25 Elastic Organic Crystals: Highly Flexible Polyhalogenated Nâ-Benzylideneanilines.
- 26 *Angewandte Chemie International Edition* **2015**, 54, (9), 2674-2678.
- 27
- 28 14. Naumov, P.; Chizhik, S.; Panda, M. K.; Nath, N. K.; Boldyreva, E., Mechanically
- 29 responsive molecular crystals. *Chemical reviews* **2015**, 115, (22), 12440-12490.
- 30
- 31 15. Chattoraj, S.; Shi, L.; Chen, M.; Alhalaweh, A.; Velaga, S.; Sun, C. C., Origin of
- 32 deteriorated crystal plasticity and compaction properties of a 1: 1 cocrystal between
- 33 piroxicam and saccharin. *Crystal Growth & Design* **2014**, 14, (8), 3864-3874.
- 34
- 35 16. Chattoraj, S.; Shi, L.; Sun, C. C., Understanding the relationship between crystal
- 36 structure, plasticity and compaction behaviour of theophylline, methyl gallate, and
- 37 their 1: 1 co-crystal. *CrystEngComm* **2010**, 12, (8), 2466-2472.
- 38
- 39 17. Hiendrawan, S.; Veriansyah, B.; Widjojokusumo, E.; Soewandhi, S. N.; Wikarsa, S.;
- 40 Tjandrawinata, R. R., Physicochemical and mechanical properties of paracetamol
- 41 cocrystal with 5-nitroisophthalic acid. *International journal of pharmaceutics* **2016**,
- 42 497, (1-2), 106-113.
- 43
- 44 18. Stahly, G. P., A survey of cocrystals reported prior to 2000. *Crystal Growth & Design*
- 45 **2009**, 9, (10), 4212-4229.
- 46
- 47 19. Babu, N. J.; Nangia, A., Solubility advantage of amorphous drugs and pharmaceutical
- 48 cocrystals. *Crystal Growth & Design* **2011**, 11, (7), 2662-2679.
- 49
- 50
- 51
- 52
- 53
- 54
- 55
- 56
- 57
- 58
- 59
- 60

- 1
2
3 20. Duggirala, N. K.; Perry, M. L.; Almarsson, Å. r.; Zaworotko, M. J., Pharmaceutical
4 cocrystals: along the path to improved medicines. *Chemical Communications* **2016**,
5 52, (4), 640-655.
6
7
8 21. Huang, N.; RodrÃguez-Hornedo, N., Effect of micellar solubilization on cocrystal
9 solubility and stability. *Crystal Growth & Design* **2010**, 10, (5), 2050-2053.
10
11 22. Krishna, G. R.; Shi, L.; Bag, P. P.; Sun, C. C.; Reddy, C. M., Correlation among
12 crystal structure, mechanical behavior, and tableability in the co-crystals of vanillin
13 isomers. *Crystal Growth & Design* **2015**, 15, (4), 1827-1832.
14
15 23. Yadav, J. A.; Khomane, K. S.; Modi, S. R.; Ugale, B.; Yadav, R. N.; Nagaraja, C. M.;
16 Kumar, N.; Bansal, A. K., Correlating single crystal structure, nanomechanical, and
17 bulk compaction behavior of febuxostat polymorphs. *Molecular pharmaceutics* **2017**,
18 14, (3), 866-874.
19
20 24. Sun, C.; Grant, D. J. W., Influence of crystal structure on the tableting properties of
21 sulfamerazine polymorphs. *Pharmaceutical research* **2001**, 18, (3), 274-280.
22
23 25. Sun, C. C., Decoding powder tableability: roles of particle adhesion and plasticity.
24 *Journal of Adhesion Science and Technology* **2011**, 25, (4-5), 483-499.
25
26 26. Khomane, K. S.; More, P. K.; Raghavendra, G.; Bansal, A. K., Molecular
27 understanding of the compaction behavior of indomethacin polymorphs. *Molecular*
28 *pharmaceutics* **2013**, 10, (2), 631-639.
29
30 27. Sarcevic, I.; Orola, L.; Veidis, M. V.; Podjava, A.; Belyakov, S., Crystal and
31 molecular structure and stability of isoniazid cocrystals with selected carboxylic acids.
32 *Crystal Growth & Design* **2013**, 13, (3), 1082-1090.
33
34 28. Lemmerer, A., Covalent assistance to supramolecular synthesis: modifying the drug
35 functionality of the antituberculosis API isoniazid in situ during co-crystallization
36 with GRAS and API compounds. *CrystEngComm* **2012**, 14, (7), 2465-2478.
37
38 29. Mashhadi, S. M. A.; Yunus, U.; Bhatti, M. H.; Tahir, M. N., Isoniazid cocrystals with
39 anti-oxidant hydroxy benzoic acids. *Journal of Molecular Structure* **2014**, 1076, 446-
40 452.
41
42 30. Oliver, W. C.; Pharr, G. M., Measurement of hardness and elastic modulus by
43 instrumented indentation: Advances in understanding and refinements to
44 methodology. *Journal of materials research* **2004**, 19, (1), 3-20.
45
46 31. M. J. Turner, J. J. M., S. K. Wolff, D. J. Grimwood, P. R. Spackman, D. Jayatilaka
47 and M. A. Spackman, CrystalExplorer17 (2017), University of Western Australia.
48 <http://hirshfeldsurface.net> **2017**, 506-506.
49
50
51
52
53
54
55
56
57
58
59
60

- 1
2
3 32. Matsuura, T.; Koshima, H., Introduction to chiral crystallization of achiral organic
4 compounds: Spontaneous generation of chirality. *Journal of Photochemistry and*
5 *Photobiology C: Photochemistry Reviews* **2005**, 6, (1), 7-24.
6
7
8 33. Koshima, H., Generation of chirality in two-component molecular crystals from
9 achiral molecules. *Journal of Molecular Structure* **2000**, 552, (1-3), 111-116.
10
11
12
13
14
15
16
17

Graphical abstract

(For table of content use only)



18
19
20
21
22
23
24
25
26
27
28
29
30
31
32
33
34
35
36
37
38
39
40
41
42
43
44
45
46
47
48 **Synopsis:** This study systematically addresses the deviation in supramolecular translation
49 in mechanical behavior from single crystal response to bulk phase mechanics. Four basic
50 molecular packing were explored having varying degrees of crystal anisotropy. In future,
51 accurate prediction of bulk aggregates of crystals may require high level of molecular
52 dynamic simulation for structure-property function mechanics.
53
54
55
56
57